Use of Surface Heat Transfer Measurements as a Flow Separation Diagnostic in a Two-Dimensional Reflected Oblique Shock/Turbulent Boundary Layer Interaction

A. Robert Porro and Warren R. Hingst
Lewis Research Center
Cleveland, Ohio

NASA

Use of Surface Heat Transfer Measurements as a Flow Separation Diagnostic in a Two-Dimensional Reflected Oblique Shock/Turbulent Boundary Layer Interaction

A. R. Porro[*] and W. R. Hingst[†]

NASA Lewis Research Center, Cleveland, Ohio

Abstract

The feasibility of using streamwise surface heat transfer measurements to detect the presence of flow separation in a two-dimensional reflected oblique shock/turbulent boundary layer interaction is reported. Surface heat transfer and static pressure data are presented for attached and separated flows for a free stream nominal Mach number range of 2.5 to 3.5 and shock generator angles of 2 to 8 degrees. The static pressure data do show the characteristic triple inflection point distribution for the strongly separated flow cases. The corresponding surface heat transfer data show unique trends that correlate well with the static pressure determination of the extent of the separated flow region. For the incipient or weakly separated flow cases, the static pressure data do not exhibit the characteristic triple inflection point distribution. However, the same trends in the heat transfer data that are seen for the strongly separated flow cases are evident for the weakly separated flows. Hence, the heat transfer data can be used to determine the extent of weakly separated flows when surface static pressure distributions often can not.

Nomenclature

c_f	skin friction coefficient
D	wind tunnel characteristic dimension (30.48 cm)
h	convective heat transfer coefficient (W/m^2 K)
L_{ref}	reference length
M_∞	free stream nominal Mach number
P_o	wind tunnel total pressure
p	static pressure
Q_o	applied heat transfer rate (W)
q_o''	applied heat flux (W/m^2)
Re/m	unit Reynolds number
T_{aw}	adiabatic wall temperature
T_o	wind tunnel total temperature
T_w	local wall temperature
u^+	non-dimensional law of the wall velocity
x	streamwise coordinate of instrumentation
x_{ref}	reference axial coordinate; locates shock generator plate leading edge relative to wind tunnel test section entrance
x_s	axial coordinate of inviscid shock impingement point on test surface
y	transverse coordinate
y^+	non-dimensional law of the wall transverse coordinate
z	spanwise coordinate
α	shock generator angle of attack
δ_o	boundary layer thickness upstream of interaction region

[*]Aerospace Engineer, Inlet, Duct, and Nozzle Flow Physics Branch.

[†]Aerospace Engineer, Inlet, Duct, and Nozzle Flow Physics Branch, Member AIAA.

Introduction

The interaction of an oblique shock wave with a turbulent boundary layer is a phenomenon commonly found in supersonic and hypersonic aircraft engine inlets. An inlet designer can make judicious use of an oblique shock system to decelerate the incoming flow and provide the necessary pressure recovery for an aircraft propulsion system. Typically, these design techniques require that the interaction of the shock wave with the boundary layer be well-behaved with no flow separation. The presence of flow separation will reduce the efficiency of the inlet system and can result in an inlet unstart in extreme cases.

In the design and test phases of an inlet development program, one must be able to recognize when flow separation is present. When intrusive flowfield measurements are not practical for these models, diagnostic instrumentation such as surface static pressure taps and surface-mounted thermocouples can be used to quantify the model performance.

The purpose of this paper is to propose some analysis methods to determine the presence of separation in a reflected oblique shock/turbulent boundary layer interaction. Particular attention will be given to the interpretation of heat transfer data for this interaction. The data analyzed were acquired by Hingst and Porro[1] in the NASA Lewis 1x1 ft. Supersonic Wind Tunnel (SWT).

Experiment

A flat plate with a sharp leading edge was used to generate an oblique shock which interacted with the

Table 1 Test Conditions.

Nominal Mach Number	Actual Mach Number	Tunnel Total Pressure, P_o, kPa	Boundary Layer Height, δ_o, mm	Skin Friction Coefficient, $c_f \times 10^3$	Per Meter Reynolds Number, Re $\times$ 10^{-6} m
2.5	2.47	172	37.33	1.49	17.4
3.0	2.98	207	29.04	1.35	16.6
3.5	3.43	241	31.67	1.14	15.1
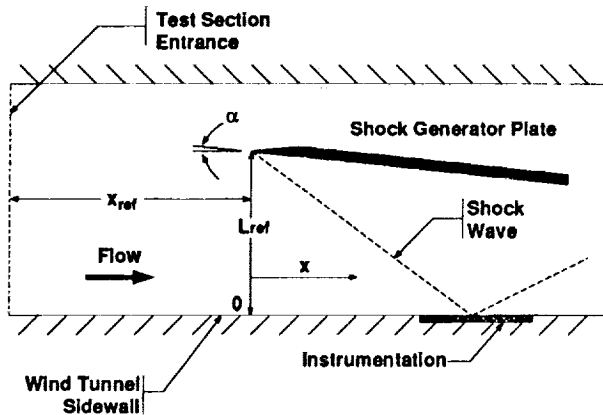
Fig. 1 Schematic of experimental hardware.

naturally-occurring sidewall turbulent boundary layer in the NASA Lewis 1x1 ft. SWT. In order to reduce three-dimensional effects, the shock generator plate spanned the entire test section, and fences were used to shield the measurement region on the wind tunnel sidewall from the corner flows at the juncture of the tunnel sidewalls. The shielding fences were located approximately 9 cm off the centerline of the wind tunnel sidewall. The shock generator plate was actuated in order to vary the incident shock angle. A schematic of the experimental hardware is shown in Fig. 1.

The test conditions of the present study along with the characteristics of the incoming turbulent boundary layers are tabulated in Table 1. Undisturbed boundary layer profile measurements were made 11.43 cm downstream of the wind tunnel test section entrance. The incoming boundary layer profiles are plotted versus a wall-wake curvefit[2] and are shown in Fig. 2. This comparison does show that the incoming boundary layers for the conditions of this study are indeed turbulent.

All quantitative measurements were made in the streamwise direction at the centerline of the wind tunnel sidewall. It is generally accepted that measurements at this location are representative of a two-dimensional interaction for moderate shock strengths. Davis and Hingst[3] have investigated the undisturbed boundary layers on the 1 x 1 ft. SWT test sidewall and have found that they are uniform and two dimensional near the spanwise center-line of the test sidewall where the measurements for the

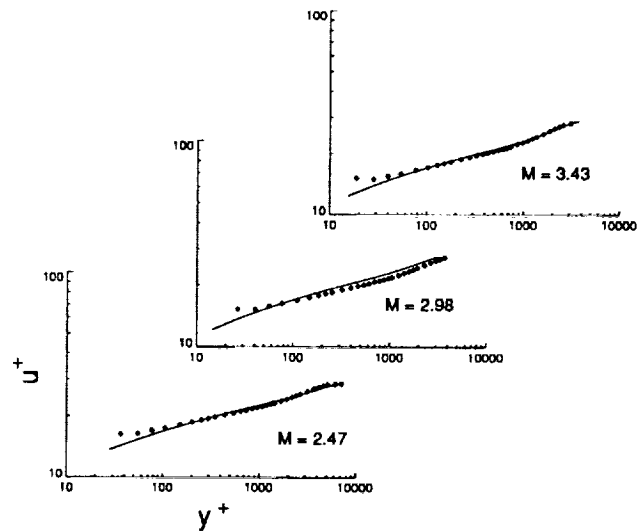present study were made. These results are depicted in Fig. 3.

Fig. 2 Wall-wake curvefit of 1x1 ft. SWT naturally-occurring boundary layers.

Removable inserts contained the appropriate instrumentation for each test phase. The first insert contained static pressure instrumentation, and the second insert had surface-mounted thermocouples on an inconel sheet. The inconel sheet was electrically isolated (insulated) so that a constant emf could be applied to the sheet. This provided an area of constant heat flux for the heat transfer measurements. The heated element area was 218.13 cm^2.

The instrumentation location coordinates were fixed relative to the wind tunnel. However, the data that will be presented subsequently were referenced to the leading edge of the shock generator plate which was not at a constant axial location throughout the testing. For some of the test conditions, the shock generator plate had to be moved a significant distance upstream so the incident oblique shock would impinge on the instrumented area of the wind tunnel sidewall. In addition, the shock generator plate did not rotate about its leading edge when the angle of attack was changed which also moved the leading edge relative to the measurement instrumentation.
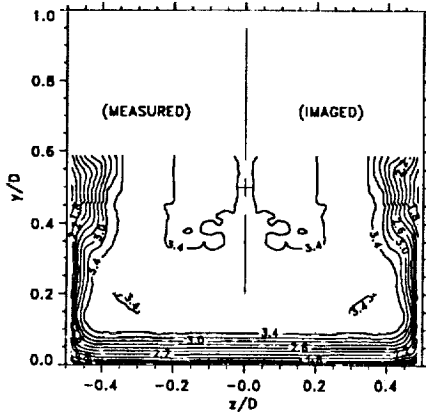
Static pressure measurements were made under nominally adiabatic tunnel wall conditions while the heat
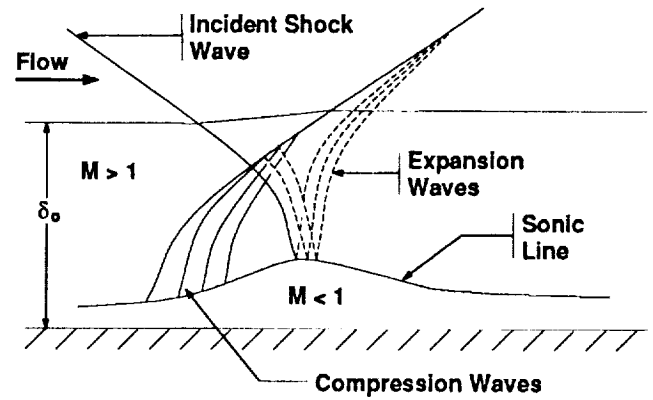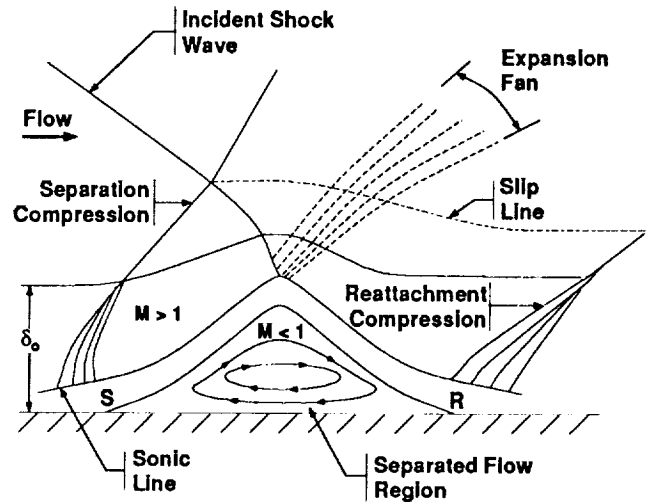
2
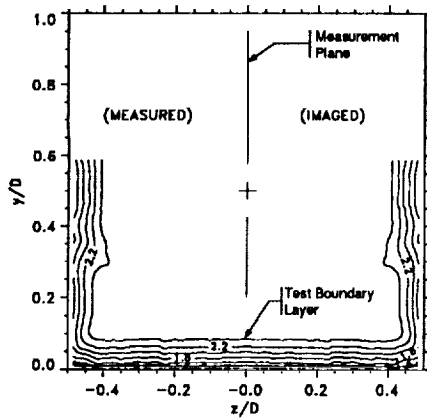
a) $M_\infty = 2.5$
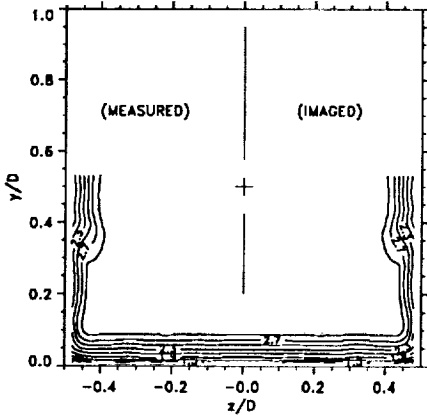
b) $M_\infty = 3.0$

c) $M_\infty = 3.5$

Fig. 3 Undisturbed boundary layers
on the NASA Lewis 1 x 1 Ft. SWT
test sidewall (adapted from ref. 3).

a) Attached flow

b) Separated flow

Fig. 4 Schematic of reflected oblique shock
wave/turbulent boundary layer interaction.

Analysis

Three types of data will be presented in this paper:
(1) schlieren flow visualization, (2) surface static pressure
measurements, and (3) heat transfer measurements. All
data were used to diagnose and determine the extent of
flow separation in the reflected oblique shock/boundary
layer interaction. An excellent discussion of the char-
acteristics of both the attached and separated reflected
oblique shock/turbulent boundary layer interaction can
be found in Ref. 4.

Schlieren Flow Visualization

Without large scale flow separation, the schlieren
will show an apparently inviscid interaction. The shock
will appear to impinge and pass through the turbulent
boundary layer and reflect from the flow surface. In real-
ity, a much more complicated process is occurring due to
the presence of the turbulent boundary layer. A schematic
of this type of interaction is shown in Fig. 4a. As the in-
cident shock passes through the boundary layer, it curves
and becomes weaker due to the transverse Mach number

transfer measurements were made with a constant heat
flux boundary condition which elevated the wall temper-
atures in the measurement region. The subsequent data
show a peak temperature rise of 12 percent above the
wind tunnel total temperature due to the heating. A de-
tailed description of the experiment can be found in Ref.
1.

3

gradient in this region. This shock wave impinges and reflects as an expansion wave in the vicinity of the boundary layer sonic line. Also, the boundary layer tends to thicken in this vicinity due to the effects of the flow compression propagating upstream through the subsonic portion of the boundary layer. This boundary layer thickening causes a series of compression waves to form upstream of the initial impingement point which then coalesce to form the reflected shock. This phenomenon manifests itself as the "upstream influence" effect in these kinds of interactions. That is, when one closely inspects the quantitative surface flow data, the effects of the impinging shock wave can be seen upstream of the actual shock impingement point.

When the shock strength increases enough to cause flow separation, the schlieren results show quite a different behavior. A schematic of this interaction is shown in Fig. 4b. In this case, a separation bubble lifts the boundary layer from the flow surface which causes a strong compression fan to form ahead of this region that again coalesces into the reflected shock wave. As the flow passes over the separation bubble, first an expansion and then a compression fan form due to the flow angularities caused by the bubble. In some instances, the schlieren may show the separation bubble itself. However, this usually needs to be substantiated by quantitative data.

Surface Static Pressure Measurements

Another method used by many researchers to detect flow separation in a reflected oblique shock/boundary layer interaction is to inspect the wall static pressure distribution in the interaction region for a triple inflection point behavior[4]. The inflection points indicate (1) separation, (2) onset of reattachment, and (3) the effect of the reattachment compression. The effect of the reattachment compression on the flow surface is believed to be the point where the flow fully reattaches to the surface. The triple inflection point diagnostic technique effectively has been used to show the extent of flow separation in a strong interaction, but is not totally effective for the case of a weak or incipient separation interaction[4]. This analysis method has been applied to the data acquired in this study, and the results will be presented subsequently.

Surface Heat Transfer Measurements

The third type of data to be analyzed for flow separation diagnostics are surface heat transfer measurements made at the spanwise centerline of the oblique shock/boundary layer interaction. Previous investigations[5-8] have acquired heat transfer data for this interaction, but only Hayashi et al.[8] have attempted to use this data as a flow separation diagnostic. Data acquired by Hingst and Porro[1] are analyzed here to further develop the use of surface heat transfer data as a means of diagnosing flow separation in a reflected oblique shock/boundary layer interaction.
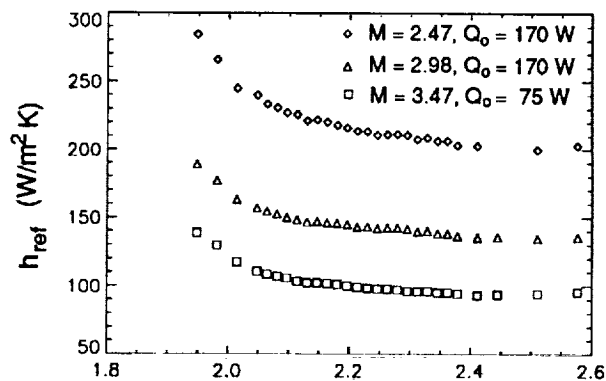
a) Convective heat transfer coefficients.
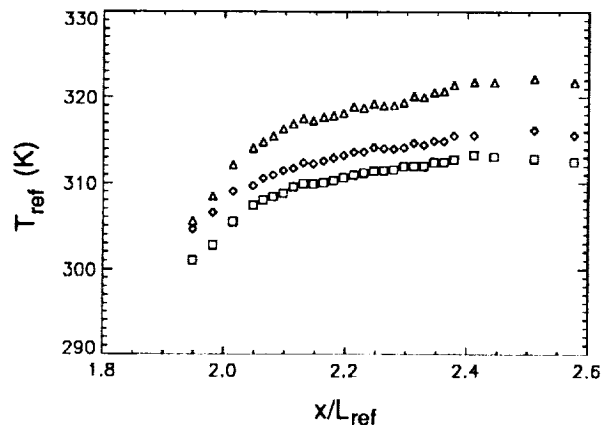
b) Temperatures.

Fig. 5 Test surface axial heat transfer and temperature distribution in the constant heat flux region.

In the experiment, a constant heat flux was applied to the flow surface in the heat transfer measurement region. Upstream of this location, the wind tunnel sidewalls were near the adiabatic wall temperature with little or no heat transfer occurring. This can be characterized as a unheated starting length problem, in which there is a step change in heat transfer on the flow surface. A temperature gradient forms as the thermal boundary layer adjusts to the new wall boundary condition. The effect of the wall heat transfer is shown in Fig. 5a. In this plot, the flow proceeds from left to right, and the strong streamwise wall convective heat transfer gradient can be seen at the beginning of the heated region. The corresponding wall temperature distribution is shown in Fig. 5b.

In order to quantify the heat transfer effects in this type of shock/boundary layer interaction, a judicious choice of data reduction is needed especially when trying to use this information to diagnose the location and extent of separated flow regions. We found that referencing the oblique shock/boundary layer interaction data to the undisturbed heated boundary layer data (cf. Fig. 5) at the same free stream conditions and applied heat flux levels yielded a good indication of flow separation. For supersonic flows, the convective heat transfer coefficient,

4

h, is defined as

$$h = \frac{q_o''}{(T_w - T_{aw})}, \qquad (1)$$

where q_o'' is the applied heat flux, T_w is the local wall temperature, and T_{aw} is the local adiabatic wall temperature. Similarly, a reference convective heat transfer coefficient can be defined as

$$h_{ref} = \frac{q_o''}{(T_{w,ref} - T_{aw})} \qquad (2)$$

where $T_{w,ref}$ is the local wall temperature for the heated, undisturbed boundary layers. Using these relations, the heat transfer for the various oblique shock/boundary layer datasets now can be referenced to the undisturbed conditions simply as the ratio, h/h_{ref}.

As an example, the raw temperature data could be presented as shown in Fig. 13b for a typical oblique shock wave/turbulent boundary layer interaction. In this case, which will be discussed in detail later, there is flow separation present, but inspection of the raw temperature distribution does not explicitly show the separation region. However, when using the analysis, the data shown in Fig. 13b are replotted as relative heat transfer coefficients which now are shown in Fig. 13c. The data now show a secondary plateau just after the shock impingement location which was not evident when inspecting the raw temperature data. This secondary plateau region is an indication of flow separation and will be discussed subsequently.

Schlieren Flow Visualization

Selected schlieren photographs of the reflected oblique shock/boundary layer interaction are shown in Figs. 6–9. The flow proceeds from left to right in these photographs. For each case, the free stream nominal Mach number is 2.5, and the shock generator angles are inclined 2, 4, 6, and 8 degrees, respectively relative to the incoming flow. In all the schlieren photos, the incident and reflected shock system appear to be quite thick or smeared. Some of this apparent smearing can be attributed to the fact that the schlieren representation of the flow field is integrated across the entire wind tunnel. Therefore, as the planar shock waves enter the sidewall boundary layers, the shock waves curve and appear to thicken due to the Mach number gradient in the sidewall boundary layers.

In addition to the incident and reflected shock, we see another disturbance in the schlieren viewing area that travels from the wind tunnel sidewall and impinges on the shock generator. This disturbance appears to be another shock wave, but it is in fact a Mach line that emanates from the juncture of the wind tunnel test section and the removable nozzles which are used to achieve the particular supersonic flow condition. The reason this Mach line seems so pronounced is because the original schlieren photographs were in color and conversion of these photographs to a black and white format have enhanced the appearance of this disturbance.
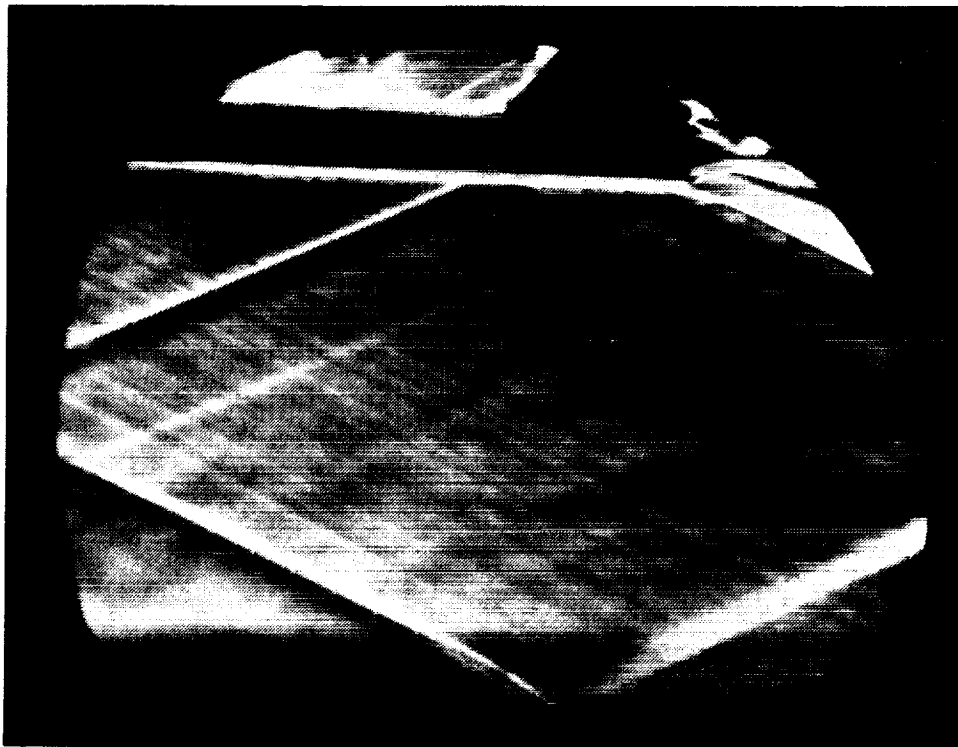

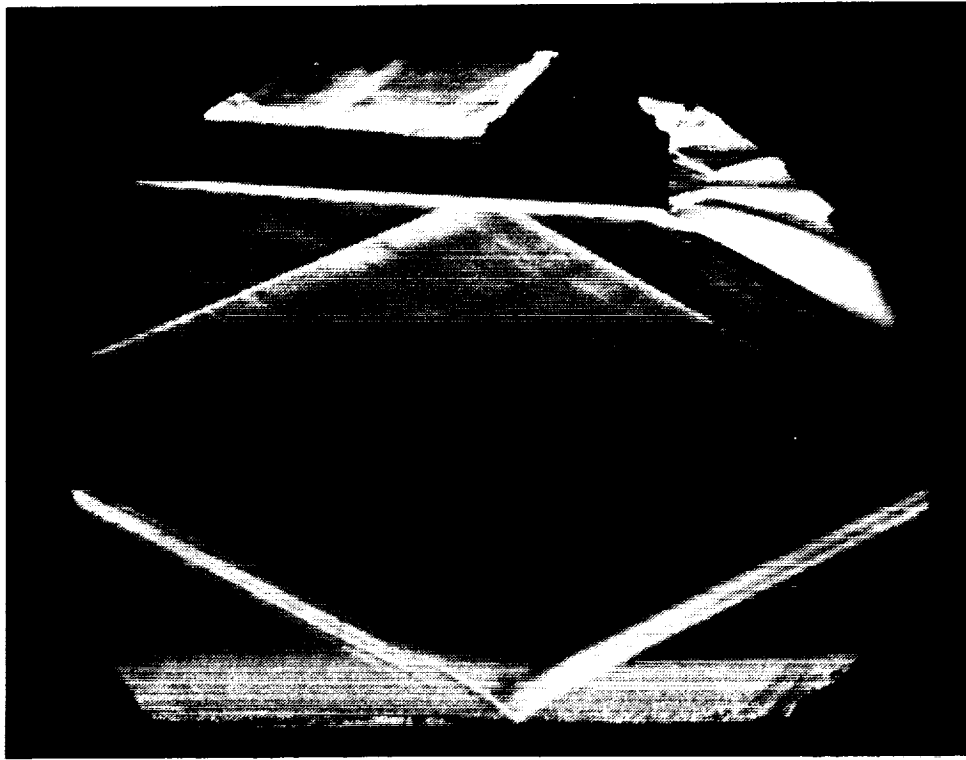**Fig. 6 Schlieren flow visualization, $M_\infty = 2.5$, $\alpha = 2.0°$.**

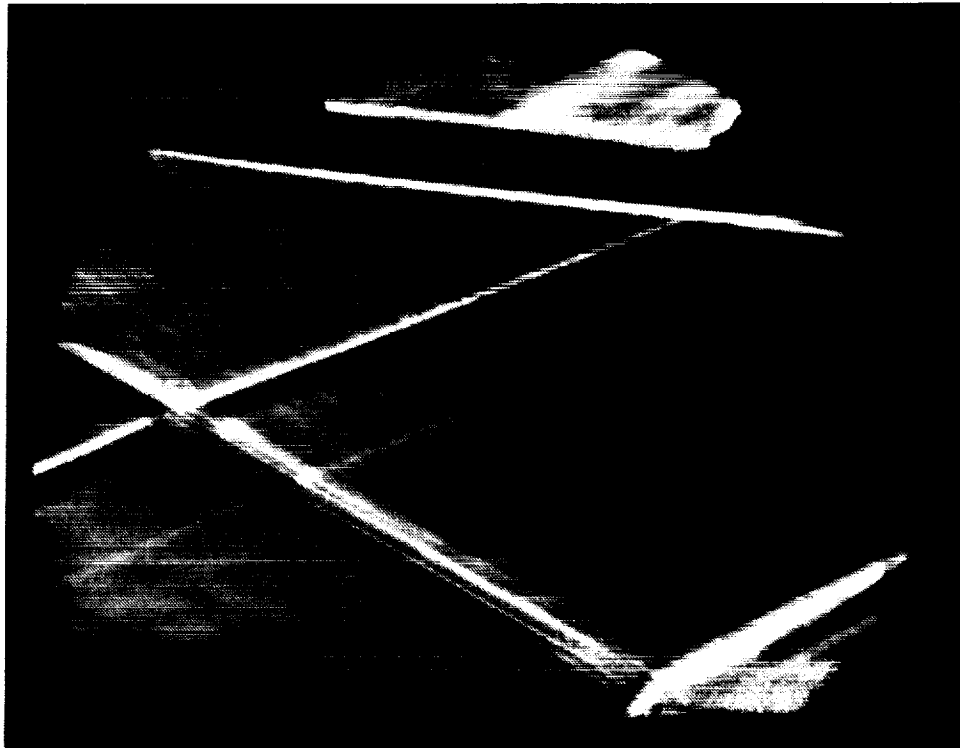Fig. 7 Schlieren flow visualization, $M_\infty = 2.5$, $\alpha = 4.0°$.

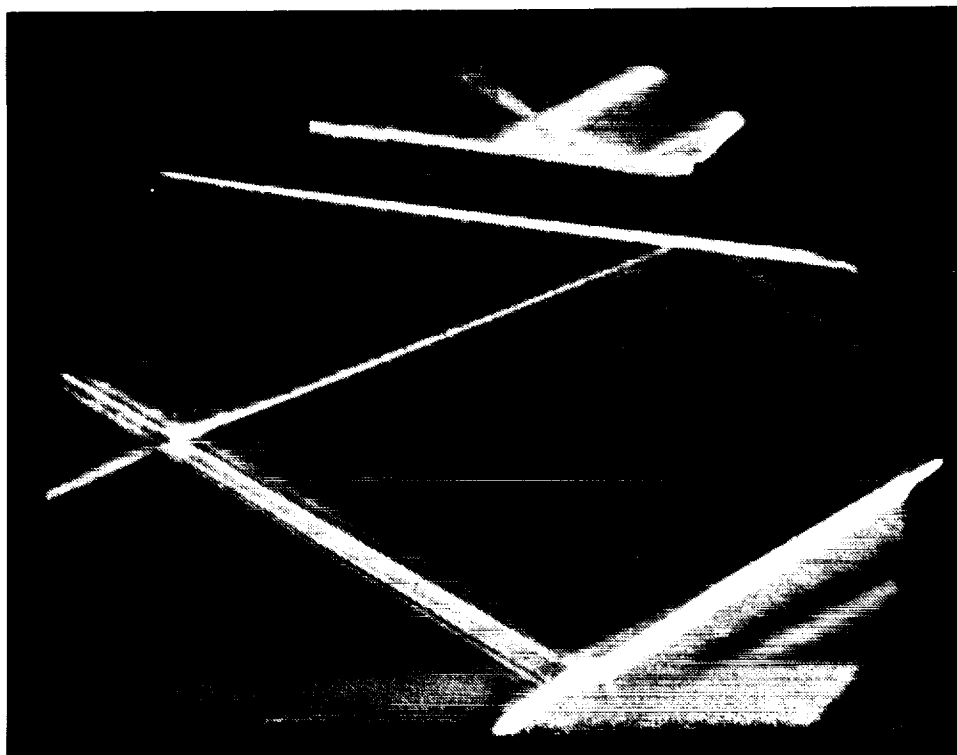Fig. 8 Schlieren flow visualization, $M_\infty = 2.5$, $\alpha = 6.0°$.

Fig. 9 Schlieren flow visualization, $M_\infty = 2.5$, $\alpha = 8.0°$.

The first two cases shown in Figs. 6 and 7 correspond to the $\alpha = 2$ and 4 degree shock generator angles and are typical schlieren results for flows that remain attached throughout the shock/boundary layer interaction region. In these figures, one can clearly see the incident shock and the corresponding reflected shock. In Fig. 7 there is also evidence of a compression fan forming just upstream of the shock impingement point.

The next two photos, Figs. 8 and 9, are the schlieren results for shock generator angles of 6 and 8 degrees, respectively and are conditions when flow separation occurs. For the 6 degree case, a casual inspection of the schlieren photograph indicates a shock structure similar to the attached flow cases. However, a closer inspection of the schlieren photograph shows evidence of the reflected shock propagating upstream of the incident shock impingement point. In reality, a small separated flow region exists, and a strong compression fan does form upstream of the incident shock due to flow angularity caused by the presence of the separation bubble. As with the attached flow cases, this compression fan coalesces to form the reflected shock.

For the 8 degree case, the separated flow region grows, and the corresponding compression fan/reflected shock system is more pronounced than what was seen for the 6 degree case. The compression fan forms farther upstream, and now evidence of an expansion fan can be seen together with the reflected shock.

A detailed inspection of Figs. 8 and 9 near the flow surface does reveal evidence of a separation bubble.

Referring to Fig. 9, one can see a dark line emanating from the base of the reflected shock and reattaching itself farther downstream of the interaction region. Correlation of this line with the static pressure and heat transfer data which will be presented subsequently shows that the line is an indication of the separated flow region. This effect can also be seen in Fig. 8 for the 6 degree case and again correlates well with the quantitative data as to the location of the separated flow region.

Surface Static Pressure Measurements

The surface static pressure distributions for all conditions considered in this study are shown in Figs. 10–19a. As with the schlieren results, the flow proceeds from left to right in these and all subsequent plots. For these particular plots, the static pressures are non-dimensionalized by a reference static pressure which corresponds to the approximate static pressure in the wind tunnel just upstream of the test hardware used in this investigation. Referring to Fig. 1, the axial distance, x, of the instrumented test surface is measured relative to the projection of the leading edge of the shock generator plate onto the flow surface, while L_{ref} is the normal distance from the test surface to the leading edge of the shock generator plate. The variable x_{ref} locates the leading edge of the shock generator plate relative to the wind tunnel test section entrance. The top axial scales in these series of plots are simply x/L_{ref}, while the bottom scales are offset relative to the calculated inviscid shock impingement

point and then are non-dimensionalized by the incoming boundary layer height, $(x-x_s)/\delta_o$.

Inspection of the static pressure data indicates that the flow does not separate for the nominal shock generator angles of 2 and 4 degrees. Flow separation does occur for shock generator angles of 6 degrees and greater. The pressure rise due to the shock impingement exceeds the theoretical inviscid pressure rise for the attached flow cases, but this overshoot becomes progressively smaller as the flow approaches separation and eventually separates. As the separation region grows due to the increasing shock strength, the static pressure rise falls below the inviscid prediction.

The location of the estimated inviscid shock impingement point on the flow surface is also shown in the static pressure distributions as the origin of the lower axial scales in the plot, i.e., $(x-x_s)/\delta_o = 0$. In all cases, the effects of the oblique shock impingement on the turbulent boundary layer can be seen upstream of the predicted inviscid shock impingement point. This is primarily due to the viscous nature of the interaction. As mentioned previously, this upstream influence effect occurs in the attached flow cases ($\alpha = 2$ and 4 degrees) because of the flow compression effects propagating upstream through the subsonic portion of the boundary layer. For the separated flow cases, the presence of the separation bubble causes a strong compression fan system to form upstream of the bubble which again manifests itself in the static pressure distributions as an upstream influence effect. In general, the initial influence effects move farther upstream relative to the inviscid shock impingement point as the shock strength increases from either increasing the free stream Mach number or the shock generator angle of attack.

The first indication of flow separation appears at the 6 degree shock generator angle for all results presented here. The separation is indicated by the two inflection points in the pressure data of Figs. 12 and 18a for the Mach 2.5 and 3.5 cases. Both inflection points are not easily seen for the Mach 3.0 case (cf. Fig. 16a) because the interaction occurred in the sparsely instrumented region of the static pressure array. The first inflection point corresponds to the location of the flow separation point. In this type of interaction, there should be three distinct inflection points in the separation region. It is not clear from the pressure data whether the second inflection point corresponds to the onset of flow reattachment or the effect of the reattachment compression wave. Other investigators[4] have noted that the triple inflection point distribution is not clearly seen when the extent of the separation region is very small.

When the shock generator angle of attack is increased to 8 degrees, the flow separation due to the oblique shock/boundary layer interaction becomes more pronounced, and the characteristic triple inflection point distribution in the pressure rise region can now be seen,

cf. Figs. 13, 17, and 19a. In each of the Figures, these inflection points are annotated and correspond to (1) the point of flow separation, (2) the onset of reattachment, and (3) the effect of the reattachment compression, respectively. The results at the 8 degree shock generator angle for the different free stream Mach numbers show that the triple inflection point distribution becomes more pronounced as the free stream Mach number and corresponding shock strength increases.

In addition to the static pressure distributions, the extent of the separation region determined by the schlieren flow visualization is shown in Figs. 12 and 13a for the Mach 2.5, $\alpha = 6$ and 8 degree cases. For the 6 degree case, the schlieren locations agree well with the static pressure results, while the schlieren overestimates the extent of the separated flow region for the 8 degree case. Since the schlieren flow visualization is integrated across the whole span of the wind tunnel, we do not expect these results to be as accurate as the quantitative measurements.

Surface Heat Transfer Measurements

The results of the surface heat transfer measurements for the oblique shock/boundary layer interaction are shown in Figs. 10–19b and c. Both the actual surface temperature measurements and inferred relative convective heat transfer distributions are presented. Each form of the data representation can give insight to the nature of flow separation in these types of interactions. The surface temperature distributions in the Figures are non-dimensionalized by the wind tunnel total temperature, T_o, while the convective heat transfer coefficients are ratioed relative to the undisturbed heated boundary layer convective heat transfer coefficients which are shown in Fig. 5.

Surface Temperature Measurements. An inspection of the data for both the attached and separated flow cases tends to show that the initial temperature gradient due to the shock impingement consistently appears downstream of the corresponding static pressure gradient.

The surface temperature measurements for the attached flow cases, $\alpha = 2$ and 4 degrees, clearly show the effect of the oblique shock impinging on the boundary layer. Near the shock impingement location, a steep gradient region appears similar to what is found in the static pressure distributions.

The temperature distributions for the separated flow cases exhibit a double peak behavior. The first peak again corresponds to the beginning of the shock/boundary layer interaction region, while the first minimum after this peak indicates the onset of flow separation (1), and the second temperature peak corresponds to the onset of flow reattachment (2). These data trends can be substantiated by comparing the wall temperature distribution to the corresponding wall static pressure distribution where the triple inflection point behavior can be seen.
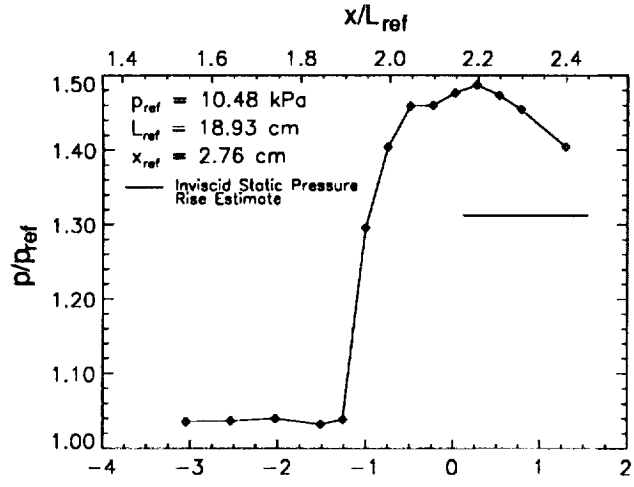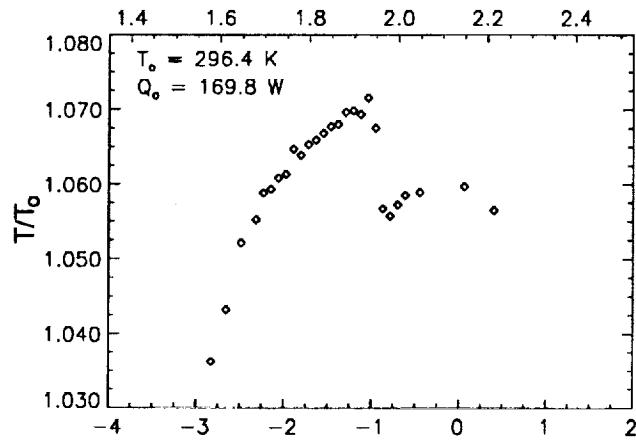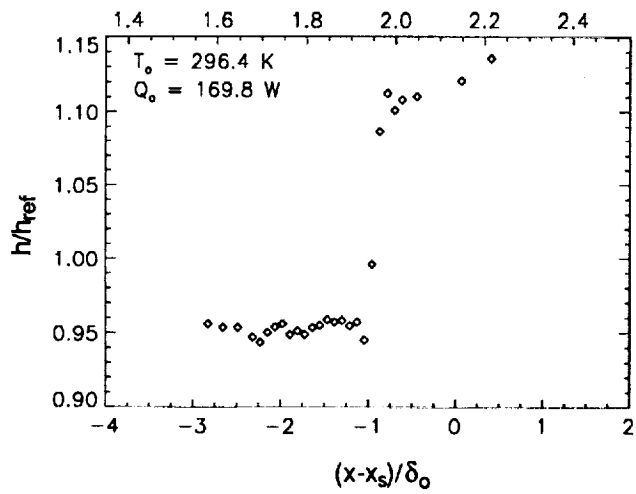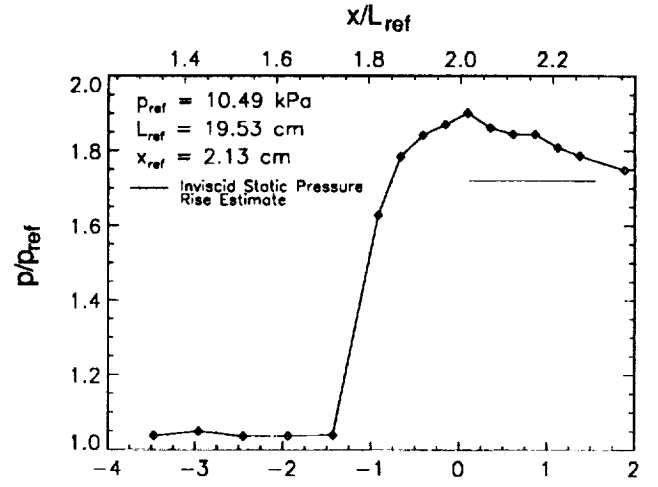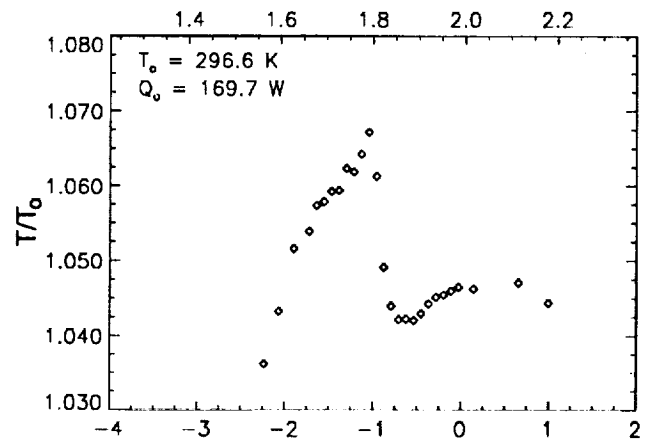
8

a) Static pressure distribution
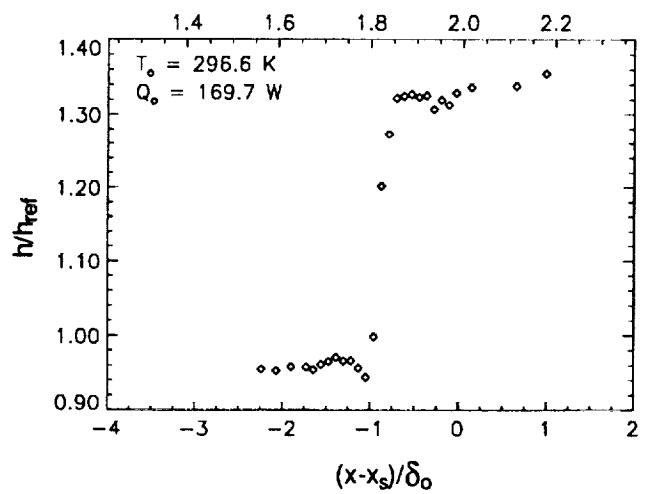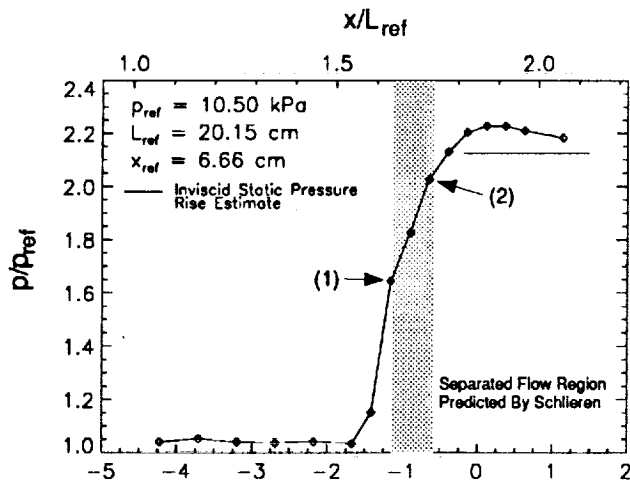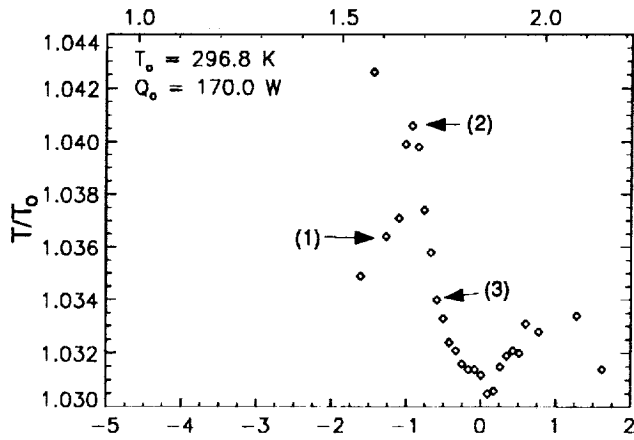
b) Surface temperature distribution

c) Relative heat transfer coefficients

Fig. 10 Effects of oblique shock on flow surface, $M_\infty = 2.5, \alpha = 2.0°$.

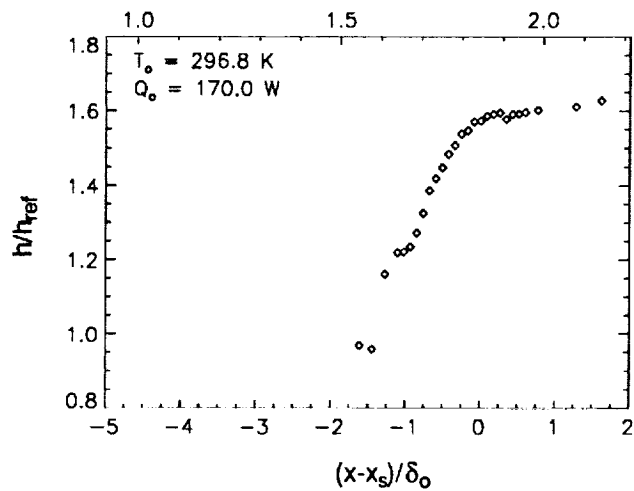a) Static pressure distribution

b) Surface temperature distribution

c) Relative heat transfer coefficients

Fig. 11 Effects of oblique shock on flow surface, $M_\infty = 2.5, \alpha = 4.0°$.
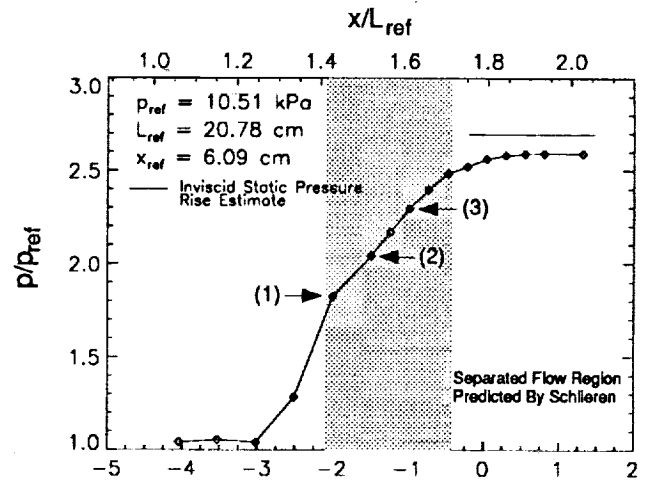
a) Static pressure distribution

b) Surface temperature distribution
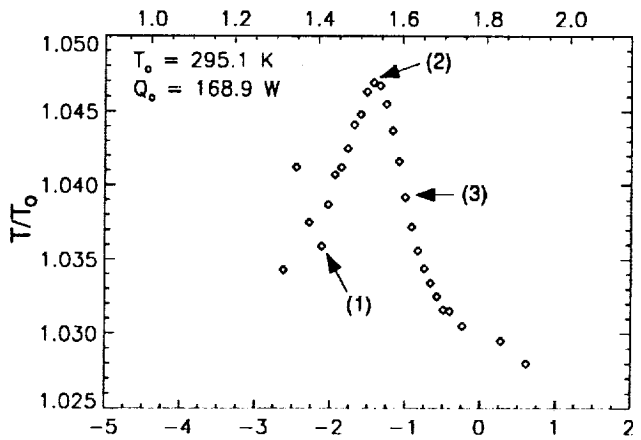

c) Relative heat transfer coefficients

Fig. 12 Effects of oblique shock on flow surface, $M_\infty = 2.5, \alpha = 6.0°$.

a) Static pressure distribution

b) Surface temperature distribution

c) Relative heat transfer coefficients

Fig. 13 Effects of oblique shock on flow surface, $M_\infty = 2.5, \alpha = 8.0°$.

a) Static pressure distribution

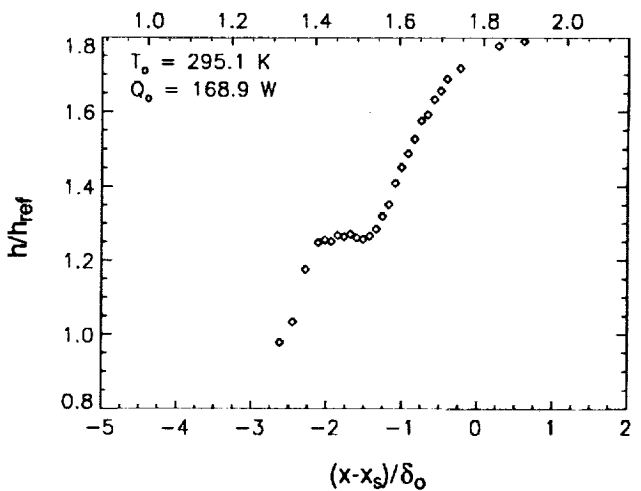b) Surface temperature distribution

c) Relative heat transfer coefficients

Fig. 14 Effects of oblique shock on
flow surface, $M_\infty = 3.0, \alpha = 2.0°$.

a) Static pressure distribution

b) Surface temperature distribution

c) Relative heat transfer coefficients
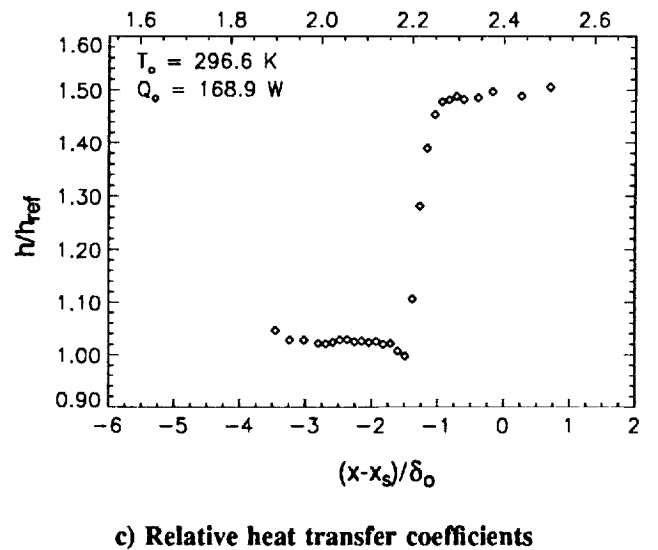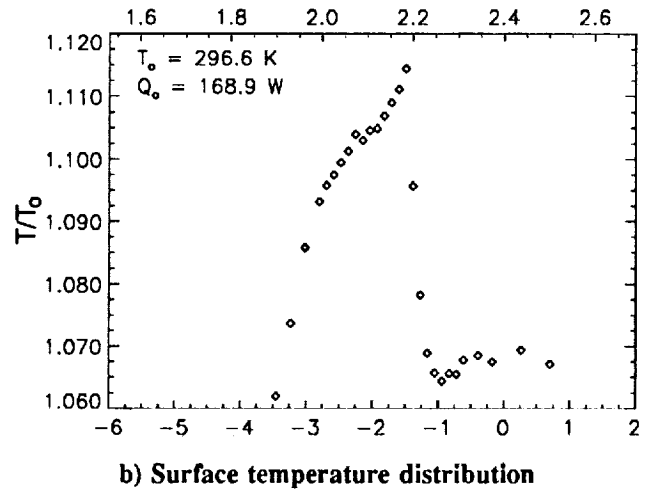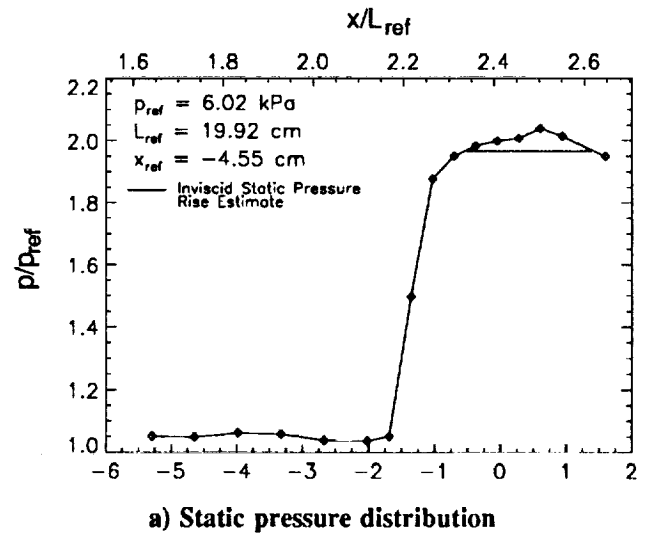
Fig. 15 Effects of oblique shock on
flow surface, $M_\infty = 3.0, \alpha = 4.0°$.
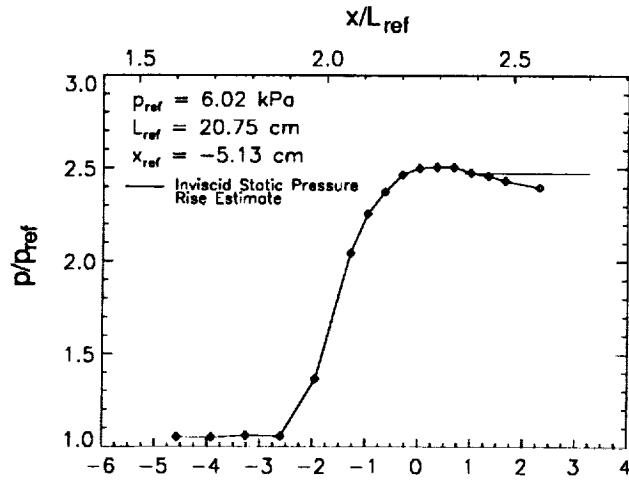
a) Static pressure distribution
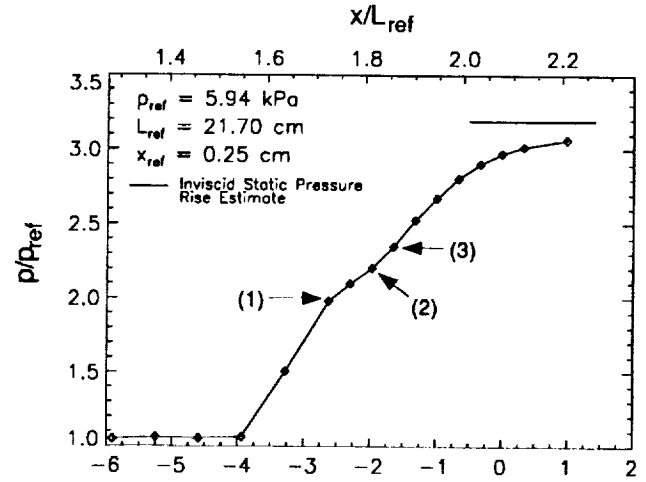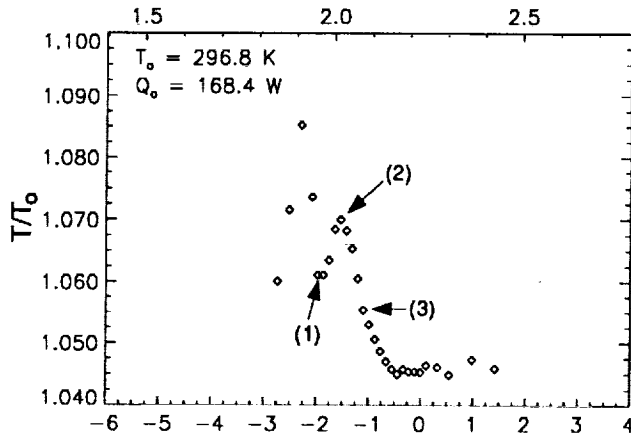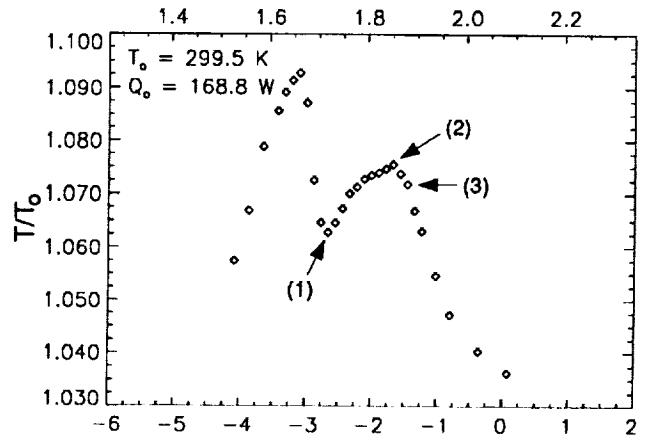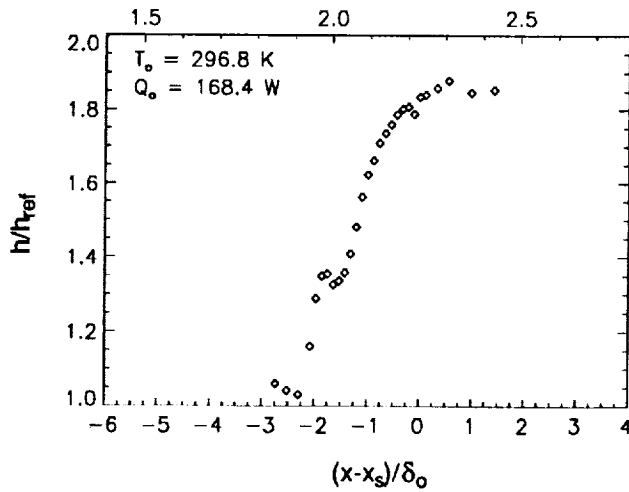
b) Surface temperature distribution
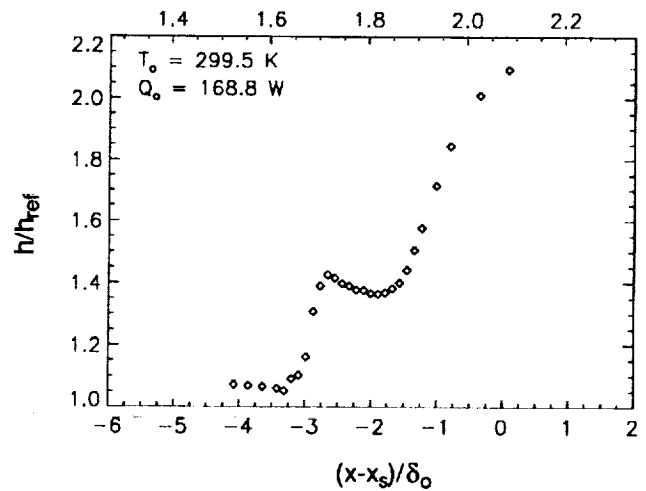
c) Relative heat transfer coefficients

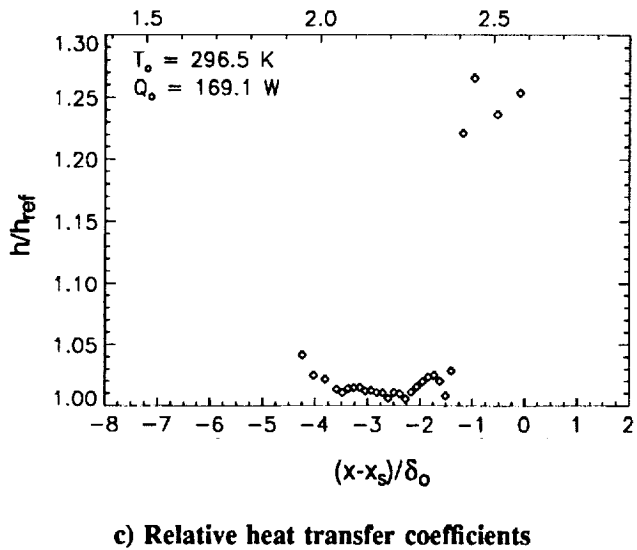**Fig. 16 Effects of oblique shock on flow surface, $M_\infty = 3.0, \alpha = 6.0°$.**

a) Static pressure distribution

b) Surface temperature distribution

c) Relative heat transfer coefficients

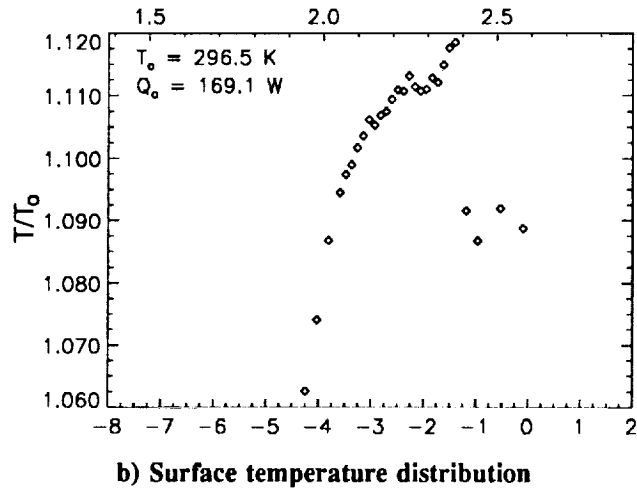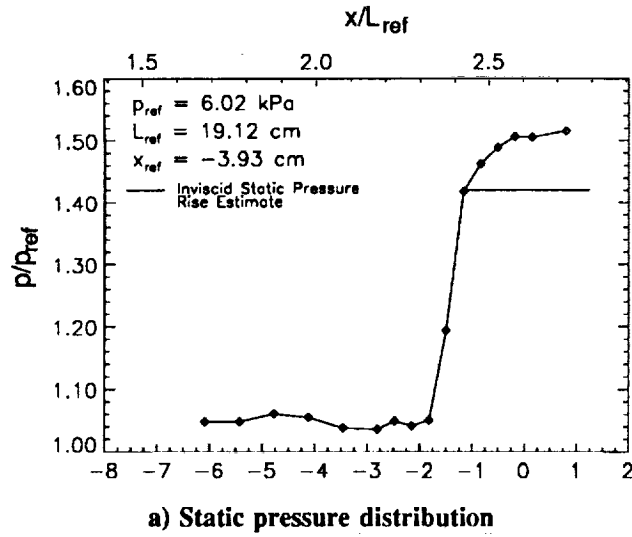**Fig. 17 Effects of oblique shock on flow surface, $M_\infty = 3.0, \alpha = 8.0°$.**
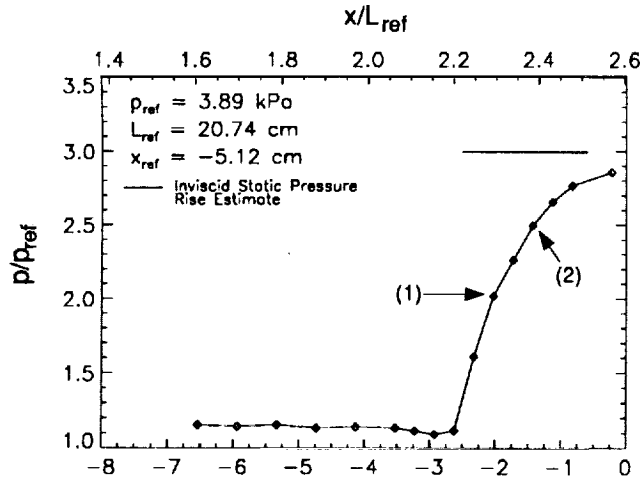
a) Static pressure distribution

b) Surface temperature distribution

c) Relative heat transfer coefficients

Fig. 18 Effects of oblique shock on
flow surface, $M_\infty = 3.5, \alpha = 6.0°$.

Fig. 19 Effects of oblique shock on
flow surface, $M_\infty = 3.5, \alpha = 8.0°$.

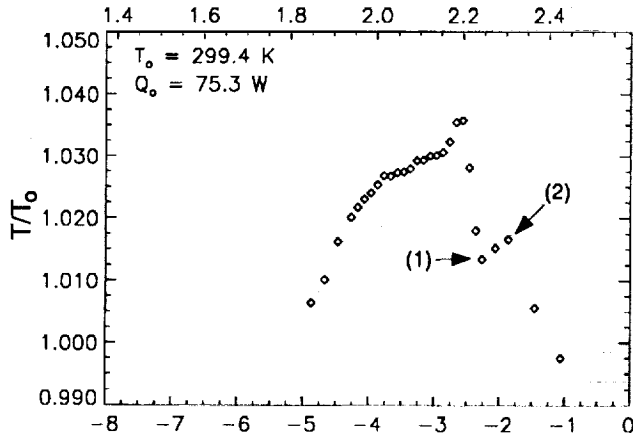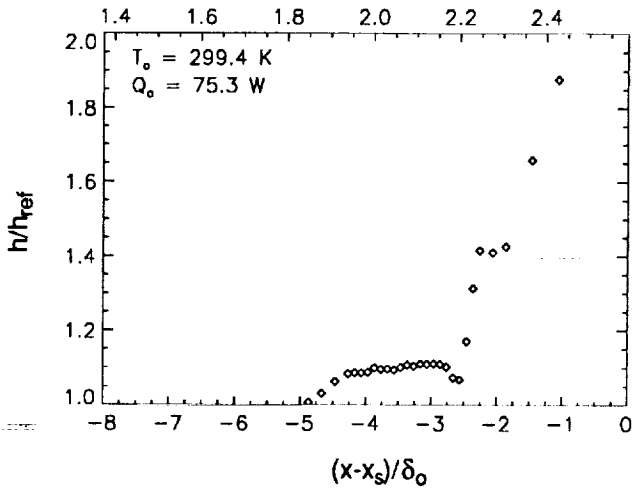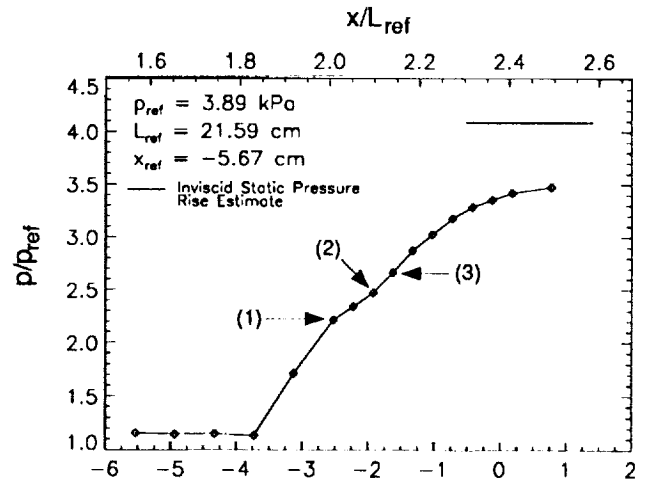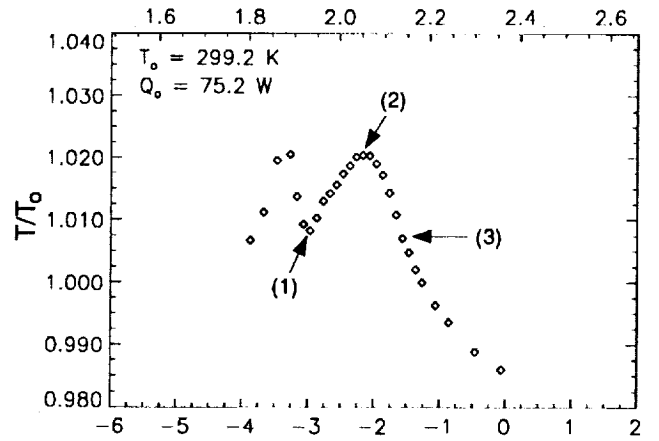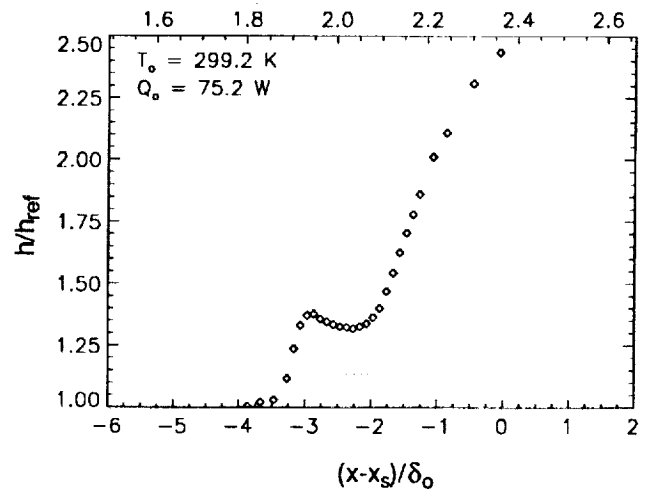For example, consider the Mach 2.5, 3.0, and 3.5, $\alpha = 8$ degree cases, Figs. 13, 17, and 19b, respectively. The first maximum in the Mach 2.5, $\alpha = 8$ degree wall temperature data does indeed correspond to the location where the initial pressure rise occurs due to the oblique shock/turbulent boundary layer interaction. The first minimum in the wall temperature distribution (1) is believed to be the boundary layer separation point. This minimum is located just upstream of the first inflection point in the wall static pressure distribution which is an alternative method to locate the flow separation point. We believe that this discrepancy between the two methods to locate the boundary layer separation point can be attributed to the sparseness of the static pressure array in this portion of the interaction region.

We feel that the secondary maximum (2) of the wall temperature distribution for the Mach 2.5, $\alpha = 8$ degree case corresponds to the onset of flow reattachment point, and this location does agree well with the second inflection point in the wall static pressure distribution. The final feature to distinguish in the wall temperature distribution is the location of the effect of the reattachment compression wave (flow reattachment point) on the temperature distribution. This is characterized by the third inflection point in the static pressure distribution. Unfortunately, there is no readily apparent feature in the wall temperature distribution such as a sharp maxima or minima to indicate this location. A perfunctory inspection of the wall temperature distribution in this region shows only a gradient region in which the wall temperature is decreasing. However, a detailed inspection of the data reveals an inflection point (3) in the gradient region which correlates reasonably well with the third inflection point in the static pressure distribution.

The Mach 3.0, $\alpha = 8$ degree results are shown in Fig. 17b. This is another separated flow case in which the static pressure distribution exhibits the characteristic triple inflection point behavior. In this case, the wall temperature distribution also shows the double peaked behavior which is seen for the Mach 2.5, $\alpha = 8$ condition. However, the Mach 3.0 data show that the first maximum in the temperature distribution, which is an indication of the extent of the upstream influence due to the shock/turbulent boundary layer interaction, occurs a significant distance downstream of the initial pressure rise. This is the only set of data for both separated and attached flows where the disagreement between the two methods used to diagnose the extent of the upstream influence becomes significant. At this time, we are not sure what causes the discrepancy at this condition.

The next feature to be seen in the wall temperature distribution at this condition is the first minimum (1) which corresponds to the flow separation point. This location correlates well with the separation location predicted by the static pressure distribution. Next appears the onset of flow reattachment point which is characterized

by the secondary maximum (2) in the wall temperature distribution. This point agrees reasonably well with the location predicted by the wall static pressure distribution.

The final feature seen in the wall temperature distribution is the first inflection point (3) in the gradient region after the secondary maximum. For the Mach 2.5, $\alpha = 8$ degree results, this inflection point corresponds to the location of the effect of the compression reattachment wave on the flow surface which correlated well with the static pressure distribution predictions. For this case, this inflection point also agrees well with the static pressure prediction of the flow reattachment point.

The Mach 3.5, $\alpha = 8$ degree results are shown in Fig. 19b. As with the previously discussed results, the surface wall temperature distribution due to the shock/turbulent boundary layer interaction exhibits the characteristic double-peaked behavior. The first peak in the temperature distribution again agrees well with the static pressure distribution as to the extent of the upstream influence effect on the flow surface. However, the first minimum, which we feel is an indication of the flow separation point, occurs upstream of the flow separation point predicted by the static pressure distribution. The secondary maximum, which we feel is the onset of flow reattachment location, again occurs slightly upstream of the location predicted by the static pressure distribution. This apparent disagreement could be due to our misinterpretation of the locations of the triple inflection points in the static pressure distribution because of insufficient static pressure data in the critical portion of the interaction region.

The final feature to be noted in the wall temperature distribution is the inflection point (3) that is indicative of the effect of the reattachment compression wave on the flow surface. This inflection point is also present in the Mach 3.5, $\alpha = 8$ degree wall temperature distribution and compares well with the corresponding static pressure prediction as to the location of the reattachment compression wave effects on the flow surface.

As mentioned previously, the static pressure distributions for the $\alpha = 6$ degree shock generator angles indicated the presence of flow separation for the free stream Mach numbers (2.5, 3.0, and 3.5) investigated in this study. However, the separated flow regions were small enough such that the limited surface static pressure instrumentation used in this study could not fully diagnose the extent of the separated flow region. That is, the static pressure distributions did reveal evidence of flow separation, but we did not clearly see the characteristic triple inflection point distribution for the $\alpha = 6$ degree cases.

In Fig. 12b, we see the surface temperature distribution for the Mach 2.5, $\alpha = 6$ degree case. The double-peaked temperature distribution is evident and can be used as a flow separation diagnostic for this interaction. As discussed before, the first peak locates the upstream influence effect of the oblique shock/turbulent boundary

14

layer interaction. This peak clearly can be seen in the plot and is in good agreement with the static pressure measurements as to the extent of the upstream influence. The first minimum (1) in the temperature distribution is indicated and corresponds to the location of the initial flow separation point. Again, this conclusion is substantiated by the first inflection point in the static pressure distribution. Next, the second maximum (2) appears in the temperature distribution which is indicative of the onset of flow reattachment point. Note that evidence of the onset of flow reattachment point cannot be readily seen in the static pressure distribution. After the flow reattachment point, we find the inflection point (3) in the downstream temperature gradient region which we have previously shown to be the effect of the reattachment compression on the flow surface. This location is in good agreement with the observed second inflection point in the surface static pressure distribution.

This same analysis can also be applied to the other 6 degree shock generator cases to diagnose flow separation. Referring to Fig. 16b, the results for a free stream Mach number of 3.0 are shown. In this particular case, the shock/boundary layer interaction occurred in the sparsely instrumented region of the static pressure array, so no definitive conclusions can be drawn as to the nature and extent of the separated flow region with these data alone. However, inspection of the surface temperature distribution reveals the location of flow separation (1), reattachment (2), and effect of the reattachment compression (3) by the methods that we discussed previously.

For the Mach 3.5, α = 6 degree condition, the static pressure distribution results shown in Fig. 18a do not easily reveal the nature and extent of the flow separation caused by the shock/boundary layer interaction. However, the surface temperature results shown in Fig. 18b do reveal some of the characteristics of the interaction, particularly the flow separation (1) and reattachment (2) locations. In this case, the interaction occurred far enough downstream such that the surface temperature data could not be used to determine the location of the effect of the reattachment compression on the flow surface.

Surface Convective Heat Transfer. The relative convective heat transfer coefficient distributions are shown in Figs. 10–19c for the conditions investigated in this study. As mentioned previously, these distributions are produced by first determining the convective heat transfer coefficient distribution for the shock/boundary layer interaction and then ratioing these results to the undisturbed heated boundary layer data (Fig. 5) at the same heating rates and free stream Mach numbers. We feel that presentation of the data in this manner gives additional insight as to the nature and extent of flow separation in a reflected oblique shock/turbulent boundary layer interaction.

The attached flow cases, free stream nominal Mach numbers of 2.5 and 3.0, α = 2 and 4 degrees, are characterized by a relatively constant relative convective heat

transfer distribution upstream of the interaction region, followed by a sharp gradient in the interaction region, and a corresponding rise in convective heat transfer levels downstream of the shock/boundary layer interaction. One feature of the heat transfer distribution that becomes apparent when the data is presented in this manner is the dip in the relative convective heat transfer coefficients just before the sharp gradient region. This trend in the convective heat transfer has been previously noted by Johnson and Kaufman II[7] and by Hayashi et al.[8] In their study, Hayashi et al. reported seeing this reduction in heat transfer before the effects of the shock/boundary layer interaction are seen in the surface static pressure distribution. Our data indicate that the beginning of this heat transfer dip appears at the same axial location where the initial static pressure rise occurs. However, as noted previously, our static pressure array was sparsely instrumented in some of the interaction region, so this could be a reason why our data do not substantiate Hayashi et al. data trends.

When flow separation occurs in the oblique shock/turbulent boundary layer interaction region, some definite trends in the relative heat transfer coefficient distribution are noted, namely a plateau region that appears in the steep gradient region that is not present with the attached flow shock/boundary layer interaction cases. For this discussion, we will consider the α = 8 degree cases for free stream nominal Mach numbers of 2.5, 3.0, and 3.5, Figs. 13, 17, and 19c.

Referring to the Mach 2.5, α = 8 degree relative convective heat transfer distribution shown in Fig. 13c, we see that the heat transfer increases in the beginning of the interaction region and then levels out to form a plateau region where the convective heat transfer is relatively constant. After this plateau region, the heat transfer again increases and forms a steep gradient region which then levels out to form another plateau at the end of the shock/boundary layer interaction region. Comparison of this data to the static pressure distribution and the surface temperature data indicate that the first plateau corresponds to the separated flow region. The initial inflection point of this plateau corresponds to the flow separation point, while the end inflection point of the plateau corresponds to the onset of flow reattachment point. The effect of the flow reattachment compression wave on the wall, which was seen in the previously presented static pressure and wall temperature distributions, is not clearly seen when the data is presented in this manner. There is evidence of an inflection point in the relative convective heat transfer coefficient distribution in the region just downstream of the separation, but it is difficult to discern whether or not it is an indication of the effect of the reattachment compression on the flow surface.

The next separated flow case, Mach 3.0 and α = 8 degrees (cf. Fig. 17), show similar trends as the Mach 2.5 data. In this case there are sufficient data points up-

stream of the interaction region that show the presence of the characteristic dip or lowering of the heat transfer coefficients in the initial portion of the shock wave/turbulent boundary layer interaction. However, this dip is not as pronounced as was observed for the attached flow results. The separated flow plateau region is evident, but it now contains a gradient region where the relative convective heat transfer decrease somewhat. Again, a comparison of this data to the corresponding wall temperature distribution data show that the first inflection point in the plateau region is the flow separation point, while the second inflection point corresponds to the onset of flow reattachment point. As with the Mach 2.5 data, the relative convective heat transfer coefficients do not clearly show evidence of the reattachment compression wave on the wall.

The Mach 3.5, α = 8 degree relative convective heat transfer coefficients are shown in Fig. 19c. The data distribution is similar to what is seen for the Mach 2.5 and 3.0 cases. Again, the separated flow plateau region can be seen along with the two inflection points that correspond to the flow separation and onset of flow reattachment points. Similar to the Mach 3.0 results, the plateau region contains a slight gradient in which the convective heat transfer decreases somewhat. As with the other separated flow relative convective heat transfer distributions, evidence of the reattachment compression effects on the wall cannot be clearly seen.

As mentioned previously for this study, the α = 6 degree shock generator cases correspond to a weakly separated oblique shock/turbulent boundary layer interaction. The heat transfer data reduced in terms of relative convective heat transfer coefficients are shown in Figs. 12, 16, and 18c for the nominal free stream Mach numbers of 2.5, 3.0, and 3.5, respectively. The characteristic dip in the convective heat transfer coefficients at the beginning of the interaction region can be seen for the Mach 3.0 and 3.5 cases. All conditions do show evidence of flow separation in the form of a plateau appearing in the steep gradient region. The separation regions are small enough so that the plateau region is not as well defined as the strongly separated flow cases discussed earlier. This introduces some ambiguity in determining the extent of the separated flow region because the two inflection points corresponding to flow separation and reattachment are not clearly visible. For these cases, it appears that the wall temperature distributions are a better flow separation diagnostic than the relative convective heat transfer coefficients.

Concluding Remarks

The ability to use surface heat transfer as a means of diagnosing the presence of flow separation in a two-dimensional reflected oblique shock/turbulent boundary layer interaction was established. The heat transfer data were compared to the streamwise centerline surface static pressure distribution in the shock/boundary layer interac-

tion region which is a widely-used flow separation diagnostic. The heat transfer data were analyzed in two forms: (1) actual surface temperature distribution, and (2) relative convective heat transfer coefficients.

The results indicate that the heat transfer data can be used as a flow separation diagnostic in a shock wave/turbulent boundary layer interaction. In general, there was good agreement between the static pressure and heat transfer data determinations of the nature and extent of the separated flow region for the strongly separated cases. The actual surface temperature rather than the relative convective heat transfer coefficients gave the best quantitative information about the extent of the separated flow region. However, from a qualitative standpoint, the relative surface convective heat transfer coefficient distribution showed the presence of flow separation much more readily than either the actual temperature or the static pressure distribution.

In the case of weak or incipient flow separation in the oblique shock/turbulent boundary layer interaction, the heat transfer data were more reliable than static pressure measurements in determining the nature and extent of the separated flow region.

References

[1] Hingst, W. R. and Porro, A. R., "Wall Static Pressue and Temperature Measurements in a Two-Dimensional Oblique Shock/Turbulent Boundary Layer Interaction," NASA publication in progress.

[2] Sun, C. C. and Childs, M. E., "Wall-Wake Velocity Profile for Compressible Nonadiabatic Flows," *AIAA Journal*, Vol. 14, June 1976, pp. 820–822.

[3] Davis, D. O. and Hingst, W. R., "Surface and Flow Field Measurements in a Symmetric Crossing Shock Wave/Turbulent Boundary Layer Interaction," AIAA Paper No. 92-2634, June 1992.

[4] Delery, J. and Marvin, J. G., "Shock-Wave Boundary Layer Interactions," AGARD AGARDograph 280, Feb. 1986.

[5] Magnam Jr., J. D. and Spurlin, C. J., "Investigation of Flow Field Interference Caused by Shock Impingement on a Flat Plate at Mach Numbers of 6, 8, and 10," AEDC TR 66-85, Apr. 1966.

[6] Gulbran, C. E., Redeker, E., Miller, D. S., and Strack, S. L., "Heating in Regions of Interfering Flow Fields Part III: Two-Dimensional Interaction Caused by Plane Shocks Impinging on Flat Plate Boundary Layers," AEDC TR 65-49, Mar. 1967.

[7] Johnson, C. B. and Kaufman II, L. G., "Interference Heating from Interactions of Shock Waves with Turbulent Boundary Layers at Mach 6," NASA TN D-7649, Sept. 1974.

[8] Hayashi, M., Sakurai, A., and Aso, S., "Meaurement of Heat-Transfer Coefficients in Shock Wave-Turbulent Boundary Layer Interaction with a Multi-Layered Thin Film Heat Transfer Gauge," NASA TM 77958, Jan. 1986.

REPORT DOCUMENTATION PAGE

Public reporting burden for this collection of information is estimated to average 1 hour per response, including the time for reviewing instructions, searching existing data sources, gathering and maintaining the data needed, and completing and reviewing the collection of information. Send comments regarding this burden estimate or any other aspect of this collection of information, including suggestions for reducing this burden, to Washington Headquarters Services, Directorate for information Operations and Reports, 1215 Jefferson Davis Highway, Suite 1204, Arlington, VA 22202-4302, and to the Office of Management and Budget, Paperwork Reduction Project (0704-0188), Washington, DC 20503.

1. AGENCY USE ONLY (Leave blank)	2. REPORT DATE	3. REPORT TYPE AND DATES COVERED
	January 1993	Technical Memorandum

4. TITLE AND SUBTITLE

Use of Surface Heat Transfer Measurements as a Flow Separation Diagnostic in a Two-Dimensional Reflected Oblique Shock/Turbulent Boundary Layer Interaction

5. FUNDING NUMBERS

WU–505–62–52

6. AUTHOR(S)

A. Robert Porro and Warren R. Hingst

7. PERFORMING ORGANIZATION NAME(S) AND ADDRESS(ES)

National Aeronautics and Space Administration
Lewis Research Center
Cleveland, Ohio 44135–3191

8. PERFORMING ORGANIZATION REPORT NUMBER

E–7505

9. SPONSORING/MONITORING AGENCY NAMES(S) AND ADDRESS(ES)

National Aeronautics and Space Administration
Washington, D.C. 20546–0001

10. SPONSORING/MONITORING AGENCY REPORT NUMBER

NASA TM–105981
AIAA–93–0775

11. SUPPLEMENTARY NOTES

Prepared for the 31st Aerospace Sciences Meeting and Exhibit sponsored by the American Institute of Aeronautics and Astronautics, Reno, Nevada, January 11–14, 1993. A. Robert Porro and Warren R. Hingst, Lewis Research Center. Responsible person, A. Robert Porro, (216) 433–5921.

12a. DISTRIBUTION/AVAILABILITY STATEMENT

Unclassified - Unlimited
Subject Category 28 34

12b. DISTRIBUTION CODE

13. ABSTRACT (Maximum 200 words)

The feasibility of using streamwise surface heat transfer measurements to detect the presence of flow separation in a two-dimensional reflected oblique shock/turbulent boundary layer interaction is reported. Surface heat transfer and static pressure data are presented for attached and separated flows for a free stream nominal Mach number range of 2.5 to 3.5 and shock generator angles of 2 to 8 degrees. The static pressure data do show the characteristic triple inflection point distribution for the strongly separated flow cases. The corresponding surface heat transfer data show unique trends that correlate well with the static pressure determination of the extent of the separated flow region. For the incipient or weakly separated flow cases, the static pressure data do not exhibit the characteristic triple inflection point distribution. However, the same trends in the heat transfer data that are seen for the strongly separated flow cases are evident for the weakly separated flows. Hence, the heat transfer data can be used to determine the extent of weakly separated flows when the surface static pressure distributions often can not.

14. SUBJECT TERMS

Compressible boundary layer flow; Shock waves

15. NUMBER OF PAGES

18

16. PRICE CODE

A03

17. SECURITY CLASSIFICATION OF REPORT	18. SECURITY CLASSIFICATION OF THIS PAGE	19. SECURITY CLASSIFICATION OF ABSTRACT	20. LIMITATION OF ABSTRACT
Unclassified	Unclassified	Unclassified	